INTERNATIONAL JOURNAL FOR NUMERICAL METHODS IN FLUIDS, VOL. 11, 317–329 (1990)

INTERACTIVE VORTEX SHEDDING FROM A PAIR OF CIRCULAR CYLINDERS IN A TRANSVERSE ARRANGEMENT

KEUN-SHIK CHANG AND CHANG-JOON SONG

Department of Mechanical Engineering, Korea Advanced Institute of Science and Technology, PO Box 150, Cheongryang, Seoul, Korea

SUMMARY

Interactive vortex shedding in the multiply connected domain formed by a pair of circular cylinders is analysed by the FEM–FDM blending technique. The vorticity–streamfunction formulation is used to solve the incompressible Navier–Stokes equations at $Re = 100$, with the time-dependent wall streamfunctions determined from the pressure constraint condition and the far-field streamfunctions from the integral series formula developed earlier by the authors. The standard Galerkin finite element method is used in the relatively small FEM subdomain and the finite difference method based on the general co-ordinate system in the rest of the flow domain. Symmetric, antisymmetric and asymmetric wake patterns are obtained confirming the earlier experimental findings. The bistable nature of the asymmetric vortex shedding as well as the intermittent drifting from one status to the other between symmetric and antisymmetric wake patterns are reported.

KEY WORDS FEM–FDM blending technique Multiply connected domain Pair of circular cylinders Symmetric, antisymmetric and asymmetric vortices Bistable nature

1. INTRODUCTION

It is well known that the vortices shed from a pair of circular cylinders in a steady uniform flow interact dynamically. The individual or combined wake behind the cylinders is therefore different from that behind an isolated circular cylinder. Zdravkovich[1] has reviewed the earlier works on related problems consisting of tandem, transverse and staggered arrangements of the cylinder pair. While the majority of the experimental researches were performed in the high-Reynolds-number range 10^3–10^5, Williamson,[2] using flow visualization methods, has studied the fluid flow behind a pair of bluff bodies in the low-Reynolds-number range 50–200.

The gap between the cylinder surfaces divided by the diameter, g^*, is known to be a very important parameter, particularly for the transverse arrangement. The wake pattern, Strohal number and lift and drag coefficients experience serious changes in this case. Historically, many researchers, including Biermann and Herrnstein,[3] Landweber,[4] Spivack[5] and Hori,[6] have observed these facts. When g^* is larger than about 5·0, virtually no interactions are generated between the two Karman vortex streets. When g^* is in the range 1·0–5·0, the two Karman vortex streets exist either in symmetric (opposite phase) or antisymmetric (same phase) form. Ishigai *et al.*,[7] Bearmann and Wadcock[8] and Williamson[2] have stated that one form can change to the other and each form is maintained for some period. When g^* is smaller than 1·0, more interesting

0271-2091/90/110317-13$06.50

Received May 1989
Revised November 1989

phenomena appear. Ishigai *et al.*,[7] Bearmann and Wadcock[8] and Williamson[2] have found that the wake behind the cylinder pair is asymmetric and the gap flow between the two cylinders is biased either upwards or downwards. They have also noticed that the biased flow in the gap is bistable and changes intermittently.

The present study has been motivated by these stimulating experiments and the earlier computational work done by the authors on vortex shedding from a circular cylinder.[9] The physical domain of the present problem is multiply connected and the geometry is rather complicated for generating the computational mesh. Grid generation techniques such as multiblock, grid embedding or patched co-ordinates found in Thomson *et al.*[10] may be considered for the finite difference purpose, but they are all subject to either grid singularity or an inefficient data interpolation procedure. Stansby[11] used the discrete vortex method to simulate the flow phenomena with two cylinders in a transverse arrangement. The discrete vortex method does not require a grid generation but depends on a potential flow calculation. Therefore this method is computationally efficient but restricted to the high-Reynolds-number range. The finite element method is known to be a very flexible tool in treating irregular geometry, but it is questionable as to the computational efficiency whether this should be the choice for the present highly unsteady computation regarding the vortex dynamics. A compromise is hence made in the present paper by blending the two techniques, the finite elements distributed in the limited highly viscous region connecting the two cylinders and the finite difference mesh obtained from arbitrary co-ordinates to be used in the rest of the computational domain. The two subdomains are overlapped only by one element width and no data interpolation is necessary owing to sharing of the same data points. In this way it was possible to obtain very smooth solutions with the FEM flexibility in the dilemma region and the FDM efficiency in the majority of the computational domain.

The vorticity–streamfunction form of the incompressible Navier–Stokes equations is used in the present computation. The wall vorticity is calculated from the field streamfunction value at each time step. On the two cylinder surfaces the streamfunctions are constant but vary with time. They are all updated at each time step through the restriction condition. Also, the far-field streamfunctions are accurately evaluated at each time step from the integral series formula developed by the authors.[12]

The present paper presents theoretical verification of the earlier phenomenological findings on interactive vortex shedding. The persistency as well as the intermittency of the symmetric and antisymmetric sheddings are computed. The bistable nature of the asymmetric vortex streets is confirmed. The time-mean lift and drag coefficients as well as the Strohal number are also presented for comparison with the results of the single cylinder.

2. NUMERICAL METHODS

Governing equations

The vorticity ζ and streamfunction ψ are governed by the equations

$$\frac{\partial \zeta}{\partial t} + \mathbf{u} \cdot \nabla \zeta = \frac{2}{Re} \nabla^2 \zeta, \tag{1}$$

$$\nabla^2 \psi = -\zeta, \tag{2}$$

where $\mathbf{u}(\mathbf{x}, t)$ is the velocity vector and the Reynolds number is based on the free stream velocity and the cylinder diameter. In the above the reference scales are the cylinder radius and the free

stream velocity. The velocity field is related to the vorticity and streamfunction as

$$\zeta = \frac{\partial v}{\partial x} - \frac{\partial u}{\partial y}, \tag{3}$$

$$u = \frac{\partial \psi}{\partial y}, \tag{4}$$

$$v = -\frac{\partial \psi}{\partial x}. \tag{5}$$

Finite element formulation

The standard Galerkin finite element method is used in part of the computational domain to solve equations (1) and (2). For the same test function $w(\mathbf{x})$ the weighted residual projections are given as

$$\int_\Omega \frac{\partial \zeta}{\partial t} w \mathrm{d}\Omega + \int_\Omega \mathbf{u} \cdot \nabla \zeta w \mathrm{d}\Omega = \frac{2}{Re} \int_\Omega \nabla^2 \zeta w \mathrm{d}\Omega, \tag{6}$$

$$\int_\Omega w \nabla^2 \psi \, \mathrm{d}\Omega = -\int_\Omega \zeta w \mathrm{d}\Omega, \tag{7}$$

where Ω is a domain in $\mathbb{R}^2$. Applying integration by parts to the Laplacian operators in the above equations and assigning the prescribed Dirichlet conditions to all boundary points, equations (6) and (7) can be rewritten as

$$\int_\Omega \frac{\partial \zeta}{\partial t} w \mathrm{d}\Omega + \int_\Omega \mathbf{u} \cdot \nabla \zeta w \mathrm{d}\Omega + \frac{2}{Re} \int_\Omega \nabla \zeta \cdot \nabla w \mathrm{d}\Omega = 0, \tag{8}$$

$$\int_\Omega \nabla \psi \cdot \nabla w \mathrm{d}\Omega - \int_\Omega \zeta w \mathrm{d}\Omega = 0. \tag{9}$$

In matrix form these equations form a system of ordinary differential equations:

$$\mathbf{M} \frac{\mathrm{d}\zeta}{\mathrm{d}t} + \mathbf{C}(\boldsymbol{\psi})\boldsymbol{\zeta} + \frac{2}{Re} \mathbf{K} \boldsymbol{\zeta} = 0, \tag{10}$$

$$\mathbf{K}\boldsymbol{\psi} - \mathbf{M}\boldsymbol{\zeta} = 0, \tag{11}$$

where $\boldsymbol{\zeta}$ and $\boldsymbol{\psi}$ are now vectors of the nodal values and matrices $\mathbf{M}$, $\mathbf{C}(\boldsymbol{\psi})$ and $\mathbf{K}$ are easily derived from equations (8) and (9). Forward differencing for the time term in the vorticity transport equation yields

$$\boldsymbol{\zeta}^{n+1} = \boldsymbol{\zeta}^n + \Delta t \mathbf{M}^{-1} \left(-\mathbf{C}(\boldsymbol{\psi}^n) - \frac{2}{Re} \mathbf{K} \right) \boldsymbol{\zeta}^n, \tag{12}$$

$$\boldsymbol{\psi}^{n+1} = \mathbf{K}^{-1} \mathbf{M} \boldsymbol{\zeta}^{n+1}, \tag{13}$$

where Δt is the time step. The values of the wall vorticity are obtained from the no-slip condition found in Roache.[13] Zero vorticity is used as the initial condition for equation (12). Since the matrices $\mathbf{M}$ and $\mathbf{K}$ are symmetric, the frontal technique, which is not iterative, can be used to solve the linear systems. Isoparametric elements with four nodes and bilinear shape functions are used.

Finite difference formulation

The governing equations (1) and (2) are written in the general co-ordinate system (ξ, η) by a transformation from (x, y) co-ordinates. The transformation of the equations is based on the formulae

$$f_x = (y_\eta f_\xi - y_\xi f_\eta)/J^2, \tag{14}$$

$$f_y = (x_\xi f_\eta - x_\eta f_\xi)/J^2, \tag{15}$$

$$\nabla^2 f = (\alpha f_{\xi\xi} - 2\beta f_{\xi\eta} + \gamma f_{\eta\eta} + \sigma f_\eta + \tau f_\xi)/J^2, \tag{16}$$

where

$$\alpha = x_\eta^2 + y_\eta^2, \tag{17}$$

$$\beta = x_\xi x_\eta + y_\xi y_\eta, \tag{18}$$

$$\gamma = x_\xi^2 + y_\xi^2, \tag{19}$$

$$\sigma = [(\alpha x_{\xi\xi} - 2\beta x_{\xi\eta} + \gamma x_{\eta\eta})y_\xi - (\alpha y_{\xi\xi} - 2\beta y_{\xi\eta} + \gamma y_{\eta\eta})x_\xi]/J, \tag{20}$$

$$\tau = [(\alpha y_{\xi\xi} - 2\beta y_{\xi\eta} + \gamma y_{\eta\eta})x_\xi - (\alpha x_{\xi\xi} - 2\beta x_{\xi\eta} + \gamma x_{\eta\eta})y_\eta]/J, \tag{21}$$

$$J = x_\xi y_\eta - x_\eta y_\xi. \tag{22}$$

Here f is an arbitrary function and all the subscripts mean derivatives. The metric coefficients and the Jacobian J are obtained by a numerical grid generation technique. Of many such techniques, that of Steger and Sorenson[14] is chosen in this study to generate the O-mesh surrounding the finite element region.

Central differencing in space and forward Euler differencing in time are used to retain compatibility with the FEM formulation:

$$\zeta^{n+1} = \zeta^n + \Delta t \left.\frac{\partial \zeta}{\partial t}\right|^n. \tag{23}$$

The far-field vorticity is taken as zero owing to its fast decay. Zero vorticity is also used as the initial condition. The finite difference form of the streamfunction equation is solved by the point-SOR method.

Streamfunction boundary conditions

In the multiply connected domain the values of the wall streamfunctions cannot be prescribed but must be calculated as part of the solution. To determine those unknown values, Sood and Elrod,[15] Tezduyar *et al.*[16] and Park and Chang[17] have paid attention to the single-valuedness of the pressure for the multiply connected domain. The equation of motion along an instantaneous streamline can be written as

$$\frac{\partial q}{\partial t} + q\frac{\partial q}{\partial s} = -\frac{1}{\rho}\frac{\partial p}{\partial s} - \nu\frac{\partial \zeta}{\partial n}, \tag{24}$$

where q is the speed along the streamline and s and n indicate tangential and normal directions to the streamline respectively. Integrating the above equation around a closed streamline, we obtain

$$-\nu \int_C \frac{\partial \zeta}{\partial n} \mathrm{d}s = \int_C \frac{\partial q}{\partial t} \mathrm{d}s, \tag{25}$$

where C is the integration contour. Along the stationary, impermeable, solid wall surface q is independent of time and we obtain the constraint

$$\int_C \frac{\partial \zeta}{\partial n} \mathrm{d}s = 0. \tag{26}$$

$\psi_{\text{wall}}(t)$ can now be calculated through this constraint.

For an open flow problem the computational far-field boundary is located at a finite distance from the solid bodies. It has been conventional that free stream values or potential flow solutions are applied for the streamfunction on the computational far-field boundary. However, it is required for accuracy reasons that the computational far-field boundary be located very far from the solid boundaries: for example, 100 radii for a vortex-shedding problem is not surprising owing to the slow logarithmic decay of the perturbed streamfunction. This is in contrast to the exponential decay of the vorticity. Sa and Chang[12] have recently developed a new integral series form of the far-field streamfunction and demonstrated its efficiency for time-dependent flow problems. The far-field streamfunction in this case is expressed as

$$\psi_{\text{far}}(\mathbf{x}) = \psi_{\text{FS}}(\mathbf{x}) - \frac{1}{2\pi} \int_S \zeta \ln|\mathbf{x}'| \, \mathrm{d}S, \tag{27}$$

$$\mathbf{x}' = \mathbf{x}_\zeta - \mathbf{x}, \tag{28}$$

where the subscripts 'far' and 'FS' mean far-field boundary and free stream respectively, S is the whole computational domain and $\mathbf{x}_\zeta$ is the position vector of a field vorticity point. Reference 12 further elaborates the integral on the right-hand side to obtain reduced expressions which are readily computable. Using this form, they demonstrated that it was possible to bring the computational boundary to a short distance from the origin. The distance in the present calculation was taken as 25 times the radius of the circular cylinders.

FEM–FDM blending technique

Since the FEM domain is embedded in the FDM domain, it is necessary to perform data exchange between the two systems. The two subdomains are overlapped as shown in Figure 1 by

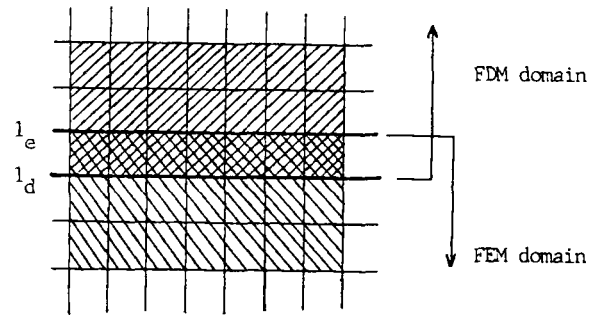

Figure 1. FEM–FDM blending

only one element width and share the same data points: hence no interpolation is necessary. During a time step advancement, the two subdomains are solved sequentially with some iterations. Thus Dirichlet boundary conditions are specified on the interface boundary in each subdomain.

In the case of the present calculation, five sub-iterations are accomplished in the FDM domain and the frontal method, which is a sort of Gauss elimination, is used in the FEM domain. This procedure completes one global iteration. In order to obtain the converged solution at each time step, several global iterations are required. The relative tolerance limit of 0·001 has been used.

3. SYMMETRIC AND ANTISYMMETRIC VORTEX SHEDDING

When the gap between the cylinder surfaces is in the range 1·0–5·0, it is known experimentally that either the symmetric or the antisymmetric vortex shedding pattern can appear. The gap and Reynolds number are chosen here as 2·0 and 100 respectively to demonstrate the appearance of these shedding patterns. The numerically generated finite difference and finite element mesh is shown in Figure 2 for two different gaps, $g^* = 2{\cdot}0$ and 0·7. The shaded closed band is the overlapped region of the two subdomains. The number of elements is 900 in the FEM subdomain and the size of the FDM mesh is 81 × 41 for a gap of 2·0. The non-dimensional time step of the computation is taken as 0·05.

Instantaneous streamlines and vorticity contours are plotted at each quarter-cycle in Figures 3 and 4. On the interface boundary between the FEM and the FDM subdomains it can be observed that the solutions are perfectly smooth. Although the cylinder pair is located normally to the free stream, each cylinder has an angle of attack because of the proximity of the two cylinders: the upper cylinder has a positive one and the lower cylinder a negative one. A repulsive force is

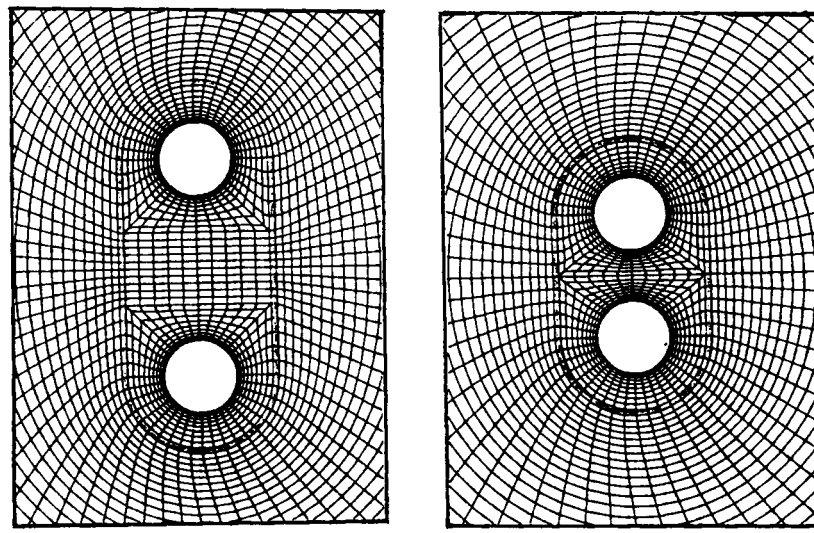

(a) (b)

Figure 2. Computational mesh: (a) $g^* = 2{\cdot}0$; (b) $g^* = 0{\cdot}7$

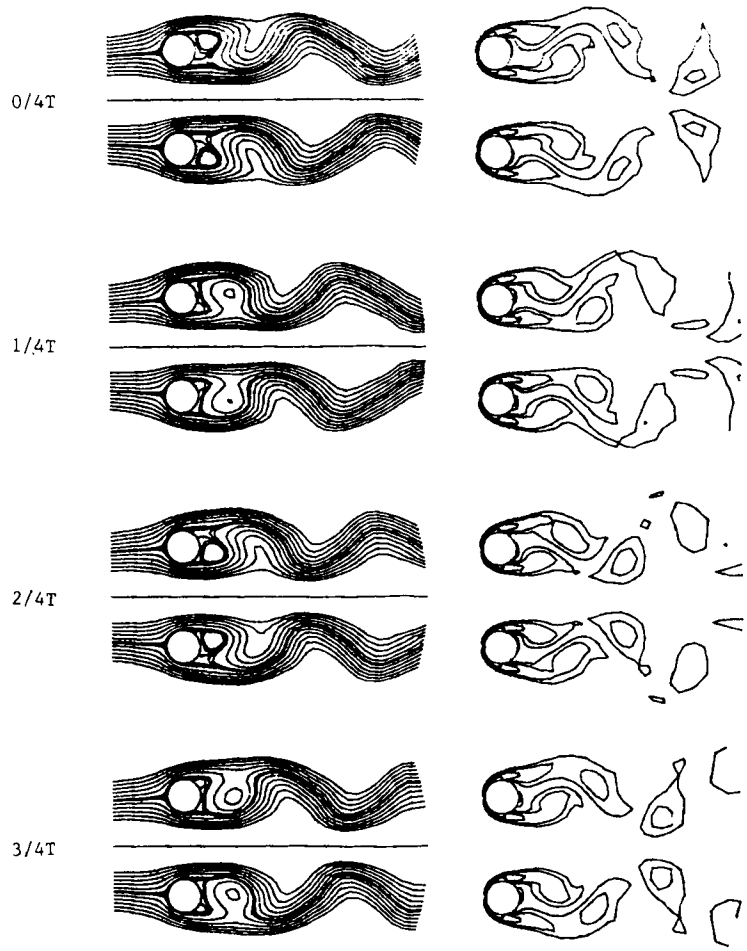

Figure 3. Symmetric vortex shedding: the instantaneous streamlines and vorticity contours

therefore created between the two cylinders in the time-mean sense. In the case of the symmetric vortex shedding (Figure 3) the vortex rows do not merge but maintain their forms for a relatively longer time span; it is noted here that the dividing streamlines are straight. In contrast, the antisymmetric vortex rows merge through a combination of vortices of the same sign, as Williamson[2] has shown using flow visualization methods; note the fluctuation of the dividing streamlines in Figure 4. In the downstream region the merged vortex rows form a single vortex street.

The curves of lift, drag and moment coefficients are shown in Figures 5 and 6. In the symmetric vortex shedding (Figure 5) the lift coefficient curves of the upper and lower cylinders have a 180° phase difference while the drag coefficient curves are almost in the same phase. In the antisymmetric case the opposite is true. It is recalled that for a circular cylinder the drag coefficient fluctuates twice during one period of alternate vortex shedding. In the case of a pair of circular cylinders, however, one period of the drag coefficient is the same as that of the lift coefficient. In

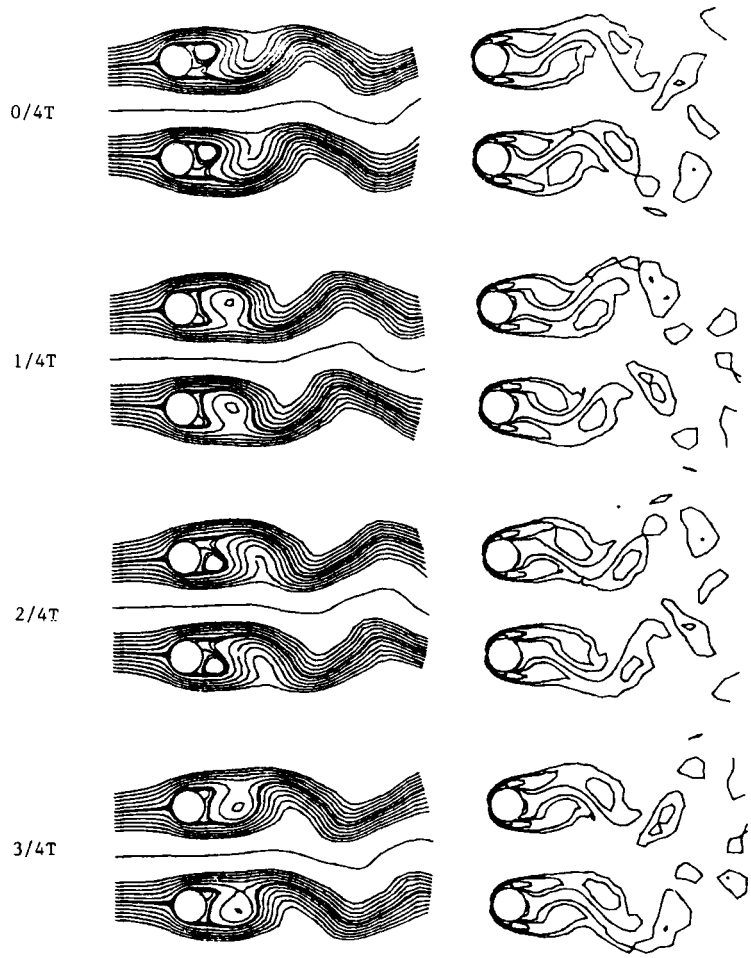

Figure 4. Antisymmetric vortex shedding: the instantaneous streamlines and vorticity contours

addition, the drag coefficient curves have three inflection points during the ascent phase but only one during the descent phase. This is attributed to the fact that the inner vortex towards the dividing streamline is somewhat smaller and weaker than the outer one during an alternate vortex shedding. It is also directly associated with the outwardly skewed position of the vortices when they are shed from each cylinder.

It is observed that the antisymmetric vortex shedding (Figure 6) has a rather regular form in the lift and drag coefficient curves in comparison with the symmetric vortex shedding. It is also ascertained in the present calculation that the former maintains its vortex pattern for a longer time span than the latter. The vortex drifts with time from the symmetric shedding to the antisymmetric one and vice versa. The process of phase change from the former to the latter is demonstrated in Figure 7.

Various fluid dynamic results from the present calculations are listed in Table I. They are the time-averaged values plus the fluctuation amplitudes during a cycle, denoted by '$\pm$' symbols.

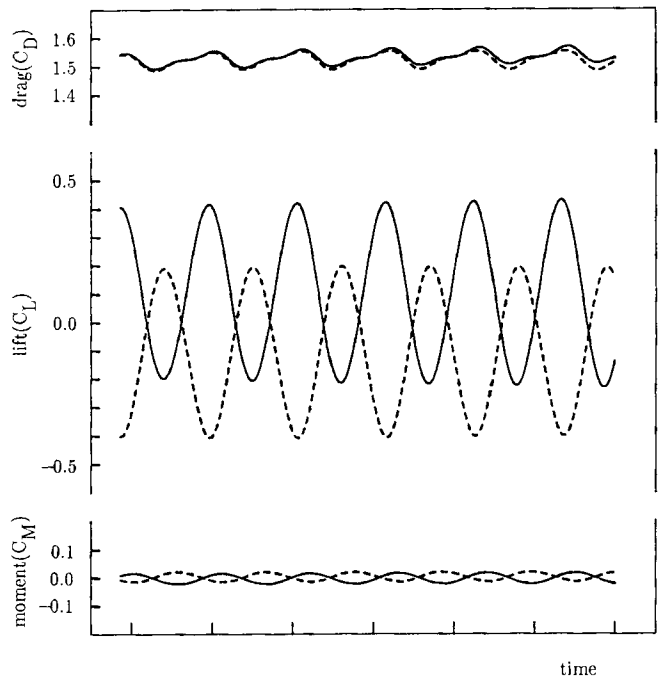

Figure 5. Lift, drag and moment coefficients for the symmetric vortex shedding; on the time axis, one division represents 20 s (the solid lines are for the upper cylinder and the dashed lines for the lower one)

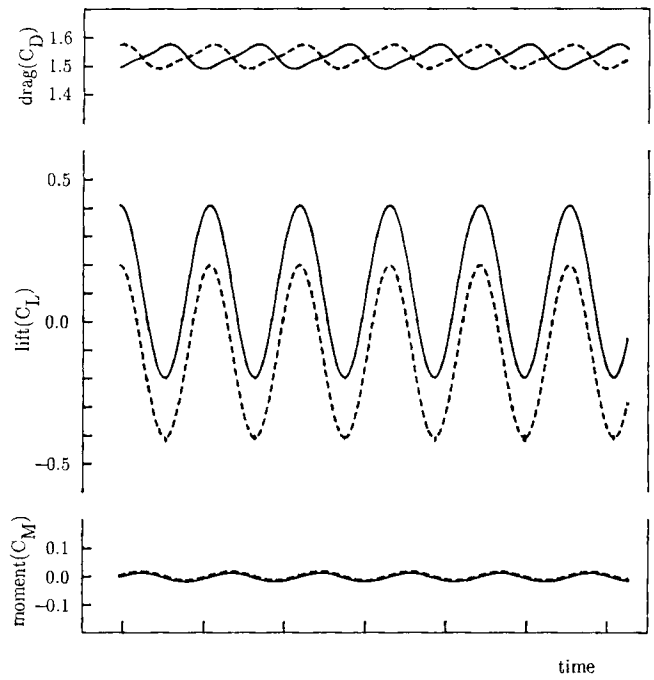

Figure 6. Lift, drag and moment coefficients for the antisymmetric vortex shedding; on the time axis, one division represents 20 s (the solid lines are for the upper cylinder and the dashed lines for the lower one)

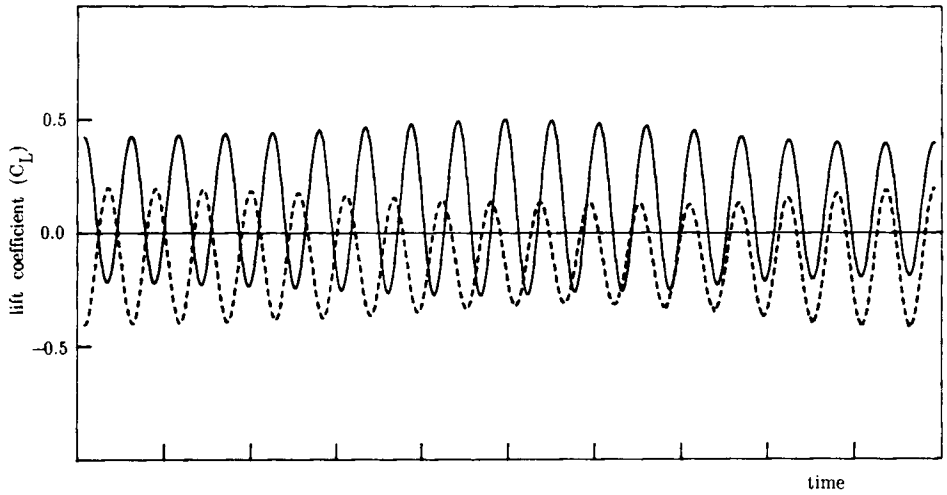

Figure 7. Drift from the symmetric vortex shedding to the antisymmetric one; on the time axis, one division represents 20 s (the solid lines are for the upper cylinder and the dashed lines for the lower one)

Table 1. Numerical results

	Case 1	Case 2	Case 3	Case 4
C_L	0·104 ± 0·31	0·108 ± 0·31	0·39	±0·26
C_D	1·525 ± 0·03	1·533 ± 0·04	0·88	1·215 ± 0·01
St	0·18	0·18	0·11, 0·22	0·16
θ_s (outside)	65·0	65·0		63·5
θ_s (inside)	57·8	58·1		63·9

Case 1: cylinder pair, $g^* = 2{\cdot}0$, symmetric vortex shedding.
Case 2: cylinder pair, $g^* = 2{\cdot}0$, antisymmetric vortex shedding.
Case 3: cylinder pair, $g^* = 0{\cdot}7$, asymmetric vortex shedding.
Case 4: single cylinder; the Strohal number is from Braza *et al.*[19] and the rest are from Borthwick.[20]

Zdravkovich[1] collected some experimental data in his review paper and concluded that the lift coefficient (C_L) increases as the gap becomes narrower and the sum of the bistable high and low drag coefficients (C_D) is always less than twice the drag coefficient of a single cylinder. The present results show the same trend. The separation angles (θ_s) measured from the rearward stagnation point are given by their absolute values. The inside separation angle is smaller than that of a single cylinder while the outside separation angle is slightly larger than that of a single cylinder. Also, we can see that the time-averaged numerical values are scarcely different between the symmetric and antisymmetric sheddings.

4. ASYMMETRIC VORTEX SHEDDING

When the gap is smaller than one diameter, it is known that the near wake of the cylinder pair is asymmetric and the gap flow is biased. In this section the representative gap is chosen as 0·7. As in the previous section, the Reynolds number based on the freestream velocity and the cylinder

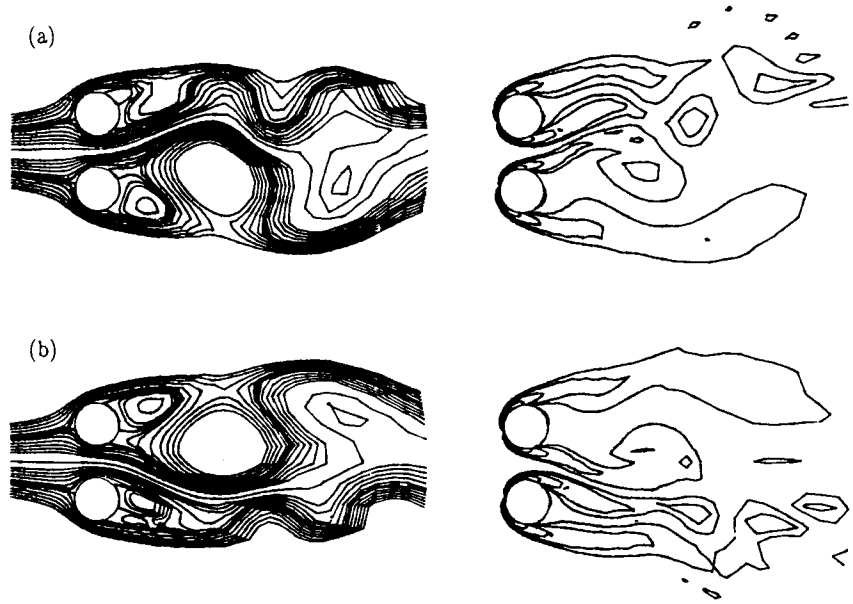

Figure 8. Instantaneous streamlines and vorticity contours for the asymmetric vortex shedding. (a) upward bias; (b) downward bias

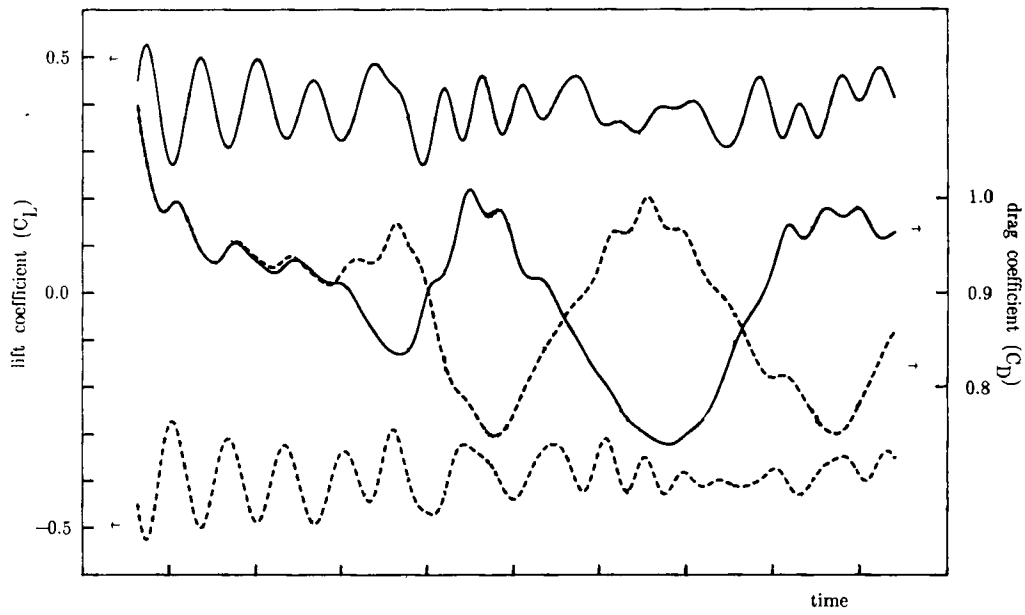

Figure 9. Lift and drag coefficients showing the bistable nature (the solid lines are for the upper cylinder and the dashed lines for the lower one)

diameter is 100. The number of elements is 780 in the FEM subdomain and the FDM mesh is 61×41. The time step is also 0·05.

The biased gap flow is clearly shown in Figure 8. The individual vortex street does not exist but the combined vortices establish a single wake as if they had originated from a single body. This is due to the fact that the velocity of the gap flow is slow and the gap vorticity is weak compared with the case of larger gap size. The calculated drag coefficient curves indeed describe the bistable nature of the wake behind the cylinder pair; see Figure 9. When the gap flow is deflected upwards, the upper cylinder has a larger drag and higher shedding frequency than the lower one since the wake behind the former is relatively in suction pressure. It is shown in the curves of lift coefficient that the higher-drag cylinder has a higher shedding frequency, about twice that of the lower-drag one. These facts are in good agreement with the many earlier experimental observations done by Ishigai *et al.*,[7] Bearmann and Wadcock[8] and Quadflieg.[18]

Case 3 of Table I shows that the asymmetric vortex shedding has two different Strohal numbers St ($=fd/U$, where f is the shedding frequency) because of its bistable nature. Actually, the Strohal numbers are somewhat scattered around the two different values separately. The experimental results of the above authors showed that the two different Strohal numbers were collected around 0·12 and 0·24 when $g^* = 0{\cdot}7$ and around 0·20 when $g^* = 2{\cdot}0$. Since they carried out their experiments in the Reynolds number range 10^3–10^5, the Strohal numbers are a little higher than the present results shown in Table I, but the bistable nature compares well.

5. CONCLUSIONS

Investigations of the flow around a pair of circular cylinders have been carried out in the literature mainly by experiments. The multiple-connectedness of the flow domain seems to have been a major handicap for a proper theoretical approach. It is evident that the finite element method can cope well with such a configuration. However, if the number of elements is large, the finite element method requires excessive computer power, especially for an unsteady flow problem. The FEM–FDM blending technique has proved to be clever practically.

The computational results showed the peculiar near-wake flow patterns such as symmetric, antisymmetric and asymmetric ones. The bistable nature of the gap flow for the asymmetric vortex shedding has been confirmed through the multiple-valued Strohal number, the semi-periodic lift and drag coefficient curves and the instantaneous streamlines. Also, we have found that the antisymmetric vortex-shedding pattern is maintained for a longer span of time than the symmetric one before it drifts away to the other form.

REFERENCES

1. M. M. Zdravkovich, 'Review of flow interference between two circular cylinders in various arrangements', *J. Fluids Eng.*, **99**, 618–633 (1977).
2. C. H. K. Williamson, 'Evolution of a single wake behind a pair of bluff bodies', *J. Fluid Mech.*, **159**, 1–18 (1985).
3. D. Biermann and W. H. Herrnstein Jr., 'The interference between struts in various combinations', *National Advisory Committee for Aeronautics, Technical Report 468*, 1933.
4. L. Landweber, 'Flow about a pair of adjacent, parallel cylinders normal to a stream', *Navy Department, D. W. Taylor Model Basin, Report 485*, 1942
5. H. M. Spivack, 'Vortex frequency and flow pattern in the wake of two parallel cylinders at varied spacings normal to an air stream', *J. Aeronaut. Sci.*, **13**, 289–297 (1946).
6. E. Hori, 'Experiments on flow around a pair of parallel circular cylinders', *Proc. 9th Japan Natl. Congr. for Applied Mechanics*, Tokyo, 1959, pp. 231–234.
7. S. Ishigai, E. Nishikawa, K. Nishimura and K. Cho, 'Experimental study on structure of gas flow in tube banks with tube axes normal to flow', *Bull. JSME*, **15**, 949–956 (1972).
8. P. W. Bearmann and A. J. Wadcock, 'The interaction between a pair of circular cylinders normal to a stream', *J. Fluid Mech.*, **61**, 499–511 (1973).

9. J. Y. Sa and K. S. Chang, 'Shedding patterns of the near-wake vortices behind a circular cylinder', *Int. j. numer. methods fluids*, in press, (1990).
10. J. F. Thomson, Z. U. A. Warsi and C. W. Mastin, *Numerical Grid Generation*, North-Holland, Amsterdam, 1985.
11. P. K. Stansby, 'A numerical study of vortex shedding from one and two circular cylinders', *Aeronaut. Q.*, **32,** 48–68 (1981).
12. J. Y. Sa and K. S. Chang, 'Far-field stream function condition for two-dimensional incompressible flows', *J. Comput. Phys.*, in press, (1990).
13. P. R. Roache, *Computational Fluid Dynamics*, Hermosa, Albuquerque, NM, 1972.
14. J. R. Steger and R. L. Sorenson, 'Automatic mesh-point clustering near a boundary in grid generation with elliptic partial differential equation', *J. Comput. Phys.* **33,** 405–410 (1979).
15. D. R. Sood and H. G. Elrod Jr., 'Numerical solution of the incompressible Navier-Stokes equations in doubly-connected regions', *AIAA J.*, **12,** 636–641 (1974).
16. T. E. Tezduyar, R. Glowinski and J. Liou, 'Petrov–Galerkin methods on multiply connected domains for the vorticity–stream function formulation of the incompressible Navier–Stokes equations', *Int. j. numer. methods fluids*, **8,** 1269–1290 (1988).
17. S. K. Park, K. S. Chang and C. E. Park, 'Interactive laminar natural convection from a pair of horizontally parallel square cylinders', *Proc. 1st Computational Fluid Dynamics Symp.*, pp. 445–448, Tokyo, 1987.
18. H. Quadflieg, 'Vortex induced load on the cylinder pair at high *Re*', *Forsch. Ing. Wes.*, **43,** 9–18 (1977).
19. M. Braza, P. Chassaing and H. H. Minh, 'Numerical study and physical analysis of the pressure and vorticity fields in the near wake of a circular cylinder', *J. Fluid Mech.*, **165,** 79–130 (1986).
20. A. Borthwick, 'Comparison between two finite difference schemes for computing the flow around a cylinder', *Int. j. numer. methods fluids*, **6,** 275–290 (1986).